

Effect of Long-Range Coulomb Interaction on NMR Shift in Massless Dirac Electrons of Organic Conductor

Yoshikazu Suzumura*

Department of Physics, Nagoya University, Nagoya 464-8602, Japan

(Received August 31, 2017; accepted November 15, 2017; published online December 28, 2017)

The nuclear magnetic resonance (NMR) shift, χ_α , at low temperatures is examined for a massless Dirac electrons in the organic conductor, α -(BEDT-TTF)₂I₃, where α [= A (= A'), B, and C] denotes the sites of the four molecules in the unit cell. The Dirac cone exists within an energy of 0.01 eV between the conduction and valence bands. The magnetic response function is calculated by taking account of the long-range Coulomb interaction and electron doping. Calculating the interaction within the first order in the perturbation, the chemical potential is determined self-consistently, and the self-energy and vertex corrections are taken to satisfy the Ward identity. The site-dependent χ_α is calculated at low temperatures of $0.0002 < T < 0.002$ (T is temperature in the unit of eV) by correctly treating the wave function of the Dirac cone. At lower (higher) temperatures the self-energy (vertex) correction of χ_α at all sites except for B is dominant and the sign is negative (positive), while the sign of the correction at the B site is always negative. For moderate doping, the shift as a function of T takes a minimum at which $\chi_C \simeq \chi_A = \chi_{A'} > \chi_B$. The relevance of the shift to the experiment is discussed.

1. Introduction

After the extensive studies on the electronic properties of low-dimensional molecular solids,¹⁾ a massless Dirac electron was found in a two-dimensional organic conductor, α -(BEDT-TTF)₂I₃,²⁾ consisting of the molecule BEDT-TTF [bis(ethylenedithio)tetrathiafulvalene], which forms a crystal with four molecules, A, A', B, and C (A = A'), in the unit cell. Using a tight-binding model with the transfer energy estimated by the extended Hückel method,^{3,4)} the massless Dirac electron is described by two valleys in the Brillouin zone where a Dirac point and Dirac cone are located between the conduction and valence bands, and a zero-gap state is realized owing to a three-quarter filled band.²⁾ The existence of the Dirac cone was verified by first-principles calculation.⁵⁾ The effect of the Dirac cone, which causes the density of states (DOS) to reduce linearly to

*E-mail: suzumura@s.phys.nagoya-u.ac.jp

zero at the energy of the Dirac point,⁶⁾ appears in both electric and magnetic properties but in a different way.⁷⁾ The linear dependence of the DOS reasonably explains the conductivity being almost constant at low temperatures, in addition to the conductivity at absolute zero temperature being close to the universal conductivity.^{8,9)} The DOS of the massless Dirac cone gives the spin susceptibility, which decreases linearly with decreasing temperature and shows the smallest (largest) value at site B (site C).¹⁰⁾ However, the calculation in terms of the tight-binding model is not enough to understand the shift of nuclear magnetic resonance (NMR),^{11,12)} since the deviation of the shift from the linear temperature dependence is large, suggesting a role of the electron correlation in the magnetic property. The detailed measurement of the NMR shift¹³⁾ suggested a noticeable effect of the interaction, although the relative magnitude of the susceptibility is compatible with that of the tight-binding model.¹⁰⁾ The subsequent theoretical work studied the role of the long-range Coulomb interaction in the shift on the basis of the renormalization of the velocity,^{14,15)} which takes account of only the self-energy of the Green function. Moreover, the wave function of the Dirac cone must be treated correctly, since the Dirac electron in α -(BEDT-TTF)₂I₃ is obtained by the four molecules per unit cell. Further, it is important to calculate the response function by treating both the self-energy and vertex corrections to satisfy the Ward identity.¹⁶⁾ In fact, the vertex correction of the spin-spin response function has been calculated for the on-site repulsive interaction,^{17,18)} where the vertex correction becomes large at high temperatures.

In the present study, we examine the NMR shift at low temperatures by taking account of the long-range Coulomb interaction and possible electron doping. The perturbational method is applied to calculate the shift since the coupling constant of the interaction is small due to a large dielectric constant in the organic conductor, as shown in the next section. In Sect. 2, the formulation is given where the wave function is treated correctly, and both self-energy and vertex corrections are calculated to satisfy the Ward identity. In Sect. 3, the solution of the chemical potential is carefully examined. The NMR shift is examined by choosing a moderate magnitude of the interaction and the doping, and the result is analyzed in terms of the self-energy and vertex corrections. In Sect. 4, we give a summary and discussion on the relevance to experiments.

2. Model and Formulation

The crystal structure of α -(BEDT-TTF)₂I₃ is shown in Fig. 1, which consists of four molecules ($\alpha = A, A', B,$ and C) in the unit cell. Transfer energies between nearest neighbor molecular sites are given by $a_1, a_2, a_3, b_1, b_2, b_3,$ and b_4 . There are also transfer energies

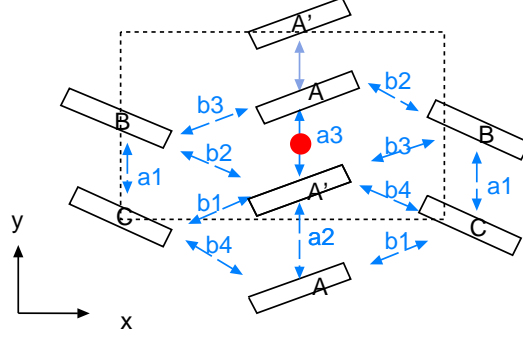


Fig. 1. (Color online) Crystal structure of α -(BEDT-TTF) $_2$ I $_3$ consisting of four molecules A, A', B and C, where the center of the unit cell (dotted square) is taken at the middle point of A and A' (closed circle). The transfer energies between nearest-neighbor molecular sites are given by bonds $a_1, a_2, a_3, b_1, b_2, b_3,$ and b_4 . There are also transfer energies between next-nearest-neighbor sites along the y -axis, and site potentials (in the main text).

between next-nearest-neighbor sites along the y -axis, where $a_{d1}, a_{d3},$ and a_{d4} correspond to A-A, B-B, and C-C, respectively. Site potentials are also added; $p_1, p_2, p_3,$ and p_4 act on the A, A', B, and C sites respectively, which come from the mean field of the short-range repulsive interaction.

We consider a Hamiltonian given by

$$H = H_0 + H_{\text{int}}, \quad (1)$$

where H_0 is the kinetic energy of a tight binding model with site potential p_α ,^{5,10)} and H_{int} denotes the long-range Coulomb interaction given by

$$H_0 = \sum_{i,j} \sum_{\alpha,\beta} \sum_{\sigma} t_{i,j;\alpha,\beta} \psi_{i,\alpha,\sigma}^\dagger \psi_{j,\beta,\sigma} + \sum_{i,\alpha} \sum_{\sigma} p_\alpha \psi_{i,\alpha,\sigma}^\dagger \psi_{i,\alpha,\sigma}, \quad (2)$$

$$H_{\text{int}} = \sum_{i,j,\alpha,\beta} \sum_{\sigma,\sigma'} \frac{e^2}{|\mathbf{r}_{i,\alpha} - \mathbf{r}_{j,\beta}|} \psi_{i,\alpha,\sigma}^\dagger \psi_{j,\beta,\sigma'}^\dagger \psi_{j,\beta,\sigma'} \psi_{i,\alpha,\sigma}. \quad (3)$$

$\psi_{i,\alpha,\sigma}^\dagger$ is the creation operator of the electron with spin σ for the molecular site α in the i -th unit cell, forming a square lattice with N and l being the total number of lattice sites and the lattice constant. $t_{i,j;\alpha,\beta}$ is the transfer energy between nearest-neighbor molecular sites. i (and j) denotes the sites of the unit cell forming a square lattice and α (and β) denotes the four molecular orbitals of A, A', B, and C. Equation (3) denotes the long-range Coulomb interaction between sites $\mathbf{r}_{i,\alpha}$ and $\mathbf{r}_{j,\beta}$. Using the Fourier transform $\psi_{\mathbf{k}\alpha,\sigma} = N^{-1/2} \sum_j \exp[-i\mathbf{k}\mathbf{r}_j] \psi_{j,\alpha,\sigma}$, where \mathbf{r}_j is a position vector on the square lattice, Eq. (2) in terms of the wave vector

$\mathbf{k} = (k_x, k_y)$ is rewritten as

$$H_0 = \sum_{\mathbf{k}} \Phi_{\sigma}(\mathbf{k})^{\dagger} \tilde{H}_0(\mathbf{k}) \Phi_{\sigma}(\mathbf{k}), \quad (4)$$

where $\Phi_{\sigma}(\mathbf{k}) = (\psi_{\mathbf{k},A,\sigma}, \psi_{\mathbf{k},A',\sigma}, \psi_{\mathbf{k},B,\sigma}, \psi_{\mathbf{k},C,\sigma})$ and $\tilde{H}_0(\mathbf{k})$ is the 4×4 matrix Hamiltonian given by

$$\tilde{H}_0(\mathbf{k}) = \begin{pmatrix} h_A & a & b & c \\ a^* & h_{A'} & d & e \\ b^* & d^* & h_B & f \\ c^* & e^* & f^* & h_C \end{pmatrix}. \quad (5)$$

The matrix elements a, \dots, f are represented in terms of transfer energies and the wave vector $\mathbf{k} = (k_x, k_y)$.¹⁰⁾ Taking an inversion center between A and A' as the origin of the unit cell and using $\tilde{k}_x = k_x l$ and $\tilde{k}_y = k_y l$, these matrix elements are given by $h_A = h_{A'} = 2a_{1d} \cos \tilde{k}_y + p_A$, $h_B = 2a_{3d} \cos \tilde{k}_y + p_B$, $h_C = 2a_{4d} \cos \tilde{k}_y + p_C$, $a = a_3 + a_2 e^{i\tilde{k}_y}$, $b = b_3 e^{-i\tilde{k}_x/2} + b_2 e^{i\tilde{k}_x/2}$, $c = b_4 e^{i(-\tilde{k}_x + \tilde{k}_y)/2} + b_1 e^{i(\tilde{k}_x + \tilde{k}_y)/2}$, $d = b_2 e^{-i\tilde{k}_x/2} + b_3 e^{i\tilde{k}_x/2}$, $e = b_1 e^{i(-\tilde{k}_x - \tilde{k}_y)/2} + b_4 e^{i(\tilde{k}_x - \tilde{k}_y)/2}$, $f = a_1 (e^{i\tilde{k}_y/2} + e^{-i\tilde{k}_y/2})$. These transfer energies in the unit of eV are given by $a_1 = 0.0267$, $a_2 = 0.0511$, $a_3 = 0.0323$, $b_1 = 0.1241$, $b_2 = 0.1296$, $b_3 = 0.0513$, $b_4 = 0.0512$, $a_{1d} = 0.0119$, $a_{3d} = 0.0046$, $a_{4d} = 0.0060$, $p_A = 1.0964$, $p_B = 1.1475$, and $p_C = 1.0997$.

The energy band $\epsilon_{\gamma}(\mathbf{k})$ [$\epsilon_1(\mathbf{k}) > \epsilon_2(\mathbf{k}) > \epsilon_3(\mathbf{k}) > \epsilon_4(\mathbf{k})$] is calculated from

$$\tilde{H}_0(\mathbf{k})|\gamma(\mathbf{k})\rangle = \epsilon_{\gamma}(\mathbf{k})|\gamma(\mathbf{k})\rangle, \quad (6a)$$

$$|\gamma(\mathbf{k})\rangle = \sum_{\alpha} d_{\alpha\gamma}|\alpha\rangle, \quad (6b)$$

where $|\gamma\rangle$ and $|\alpha\rangle$ denote the wave functions corresponding to the energy band (eigenvalue) and the lattice site, respectively. $\sum_{\alpha} d_{\alpha\gamma}(\mathbf{k})^* d_{\alpha\gamma'}(\mathbf{k}) = \delta_{\gamma,\gamma'}$ and $\sum_{\gamma} d_{\alpha\gamma}(\mathbf{k})^* d_{\beta\gamma}(\mathbf{k}) = \delta_{\alpha,\beta}$. The component of the wave function $d_{\alpha\gamma}(\mathbf{k})$, which is characteristic of α -(BEDT-TTF)₂I₃, is associated with the topological property of the wave function.¹⁹⁾ Although such a property also exists in graphene, the novel features of the present case arise from the interference effect of the four kinds of $d_{\alpha\gamma}(\mathbf{k})$ in the perturbational calculation of the NMR shift as shown later. The Dirac point, which is located between the conduction and valence bands [i.e., $\epsilon_1(\mathbf{k})$ and $\epsilon_2(\mathbf{k})$], is given by $\mathbf{k}_D/(\pi/l) = \pm(0.683, 0.440)$, corresponding to two valleys, and leads to a zero gap state due to the three-quarter-filled band.

By taking account of the screening, Eq. (3) within the random phase approximation (RPA)

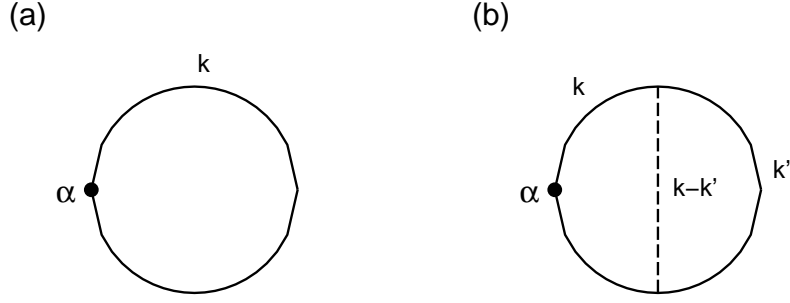


Fig. 2. Diagram for the density of zeroth order $n^{(0)}$ (a) and first order $n^{(1)}$ (b), where the summation of α is taken. The solid line denotes the one-particle Green function $(i\omega_n + \mu - \epsilon_\gamma(\mathbf{k}))^{-1}$, where $\omega_n (= (2n + 1)\pi T)$ is the Matsubara frequency with n being an integer. The dashed line denotes the RPA-screened interaction $v_{\mathbf{q},\text{eff}}$ given by Eq. (7b).

is rewritten as (Appendix A)

$$H_{\text{int}} = \frac{1}{Nl^2} \sum_{\mathbf{k}_1, \mathbf{k}_2, \mathbf{q}} \sum_{\alpha, \beta} \sum_{\sigma, \sigma'} v_{\mathbf{q},\text{eff}} \times \psi_{\mathbf{k}_1 - \mathbf{q}, \sigma}^\dagger \psi_{\mathbf{k}_2 + \mathbf{q}, \sigma'}^\dagger \psi_{\mathbf{k}_2, \sigma'} \psi_{\mathbf{k}_1, \sigma}, \quad (7a)$$

$$v_{\mathbf{q},\text{eff}} = \frac{gl}{|\mathbf{q}| + q_{\text{TF}}}, \quad (7b)$$

where $g = 2\pi e^2/(l\epsilon)$, $\epsilon = \epsilon_1\epsilon_2$. Here the intralayer and interlayer dielectric constants are given by $\epsilon_1 = (1 + 1.43e^2/v)$ and $\epsilon_2 [\sim o(10)]$, respectively. The latter is introduced owing to the layered system and is taken as a parameter since ϵ_2 is known only for the insulating state.²⁰⁾ e is the electronic charge. For $l \simeq 10 \text{ \AA}$, which is the length of the lattice constant, $2\pi e^2/l \simeq 8.5 \text{ eV}$, $v/l \simeq 0.05 \text{ eV}$, and $e^2/v \simeq 27$, with v being the averaged velocity of the Dirac cone. For $\epsilon_2 \simeq 5$, the coupling constant is estimated as $g = 0.04 \text{ eV}$, which is used in the numerical calculation. Note that the dielectric constant in the present case, $\epsilon \simeq 200$, is much larger than that of the graphene, $\epsilon \simeq 4$, with $e^2/v = 2.2$.¹⁴⁾ Since we examine the chemical potential away from the Dirac point, we introduce a quantity $q_{\text{TF}}(\delta\mu, T)$ which is the Thomas–Fermi screening constant given by (Appendix A)

$$q_{\text{TF}} = \frac{4e^2/v}{\epsilon(1 - \lambda^2)^{3/2}} \times \frac{|\delta\mu| + T}{v}, \quad (7c)$$

where $\delta\mu = \mu - \mu_0$ and μ_0 denotes μ at $g = 0$ and $T = 0$. In deriving Eq. (7c), we used a 2×2 effective Hamiltonian with the tilting parameter of the Dirac cone, $\lambda = 0.8$. In Eq. (7a), we take $|\mathbf{q} \cdot (\mathbf{r}_{i,\alpha} - \mathbf{r}_{i,\beta})| = 0$ owing to the long-range Coulomb interaction. We calculate H_{int} with a coupling constant g (in the unit of eV) up to the first order in the perturbation.

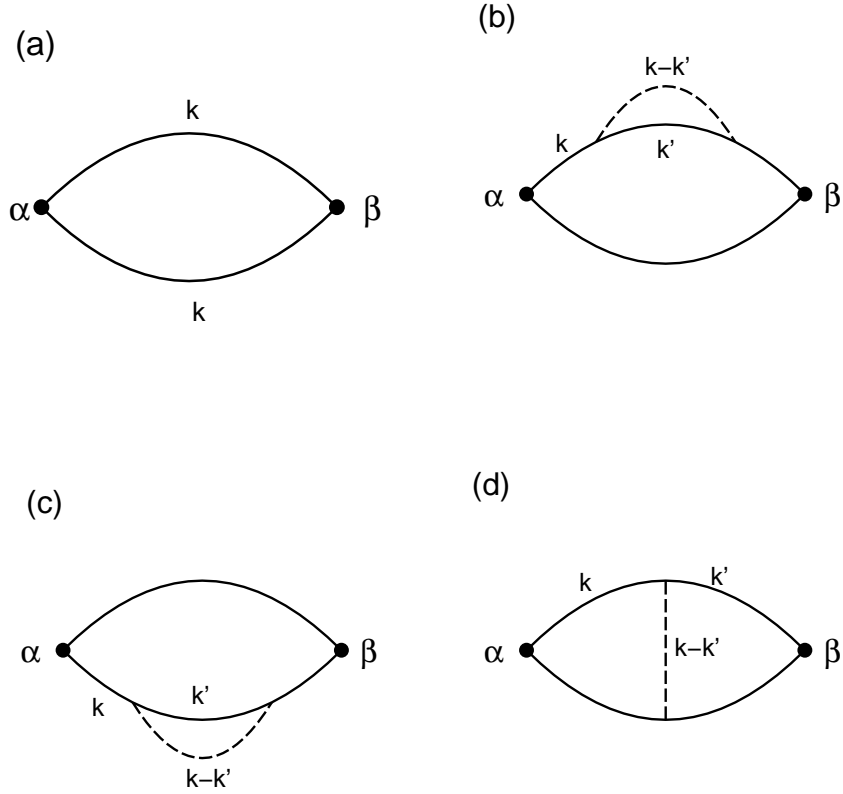


Fig. 3. Diagram of the response function for the zeroth order (a), the first order of the self-energy correction (b), (c), and the vertex correction (d). Notations are the same as in Fig. 2.

The number density per spin up to the first order of the perturbation of H_{int} is given by $n^{(0)} + g n^{(1)}$, where $n^{(0)}$ and $n^{(1)}$ are respectively shown in Figs. 2(a) and 2(b), and are calculated as (Appendix B)

$$n^{(0)} = \frac{1}{N} \sum_{\mathbf{k}} \sum_{\gamma=1}^4 f(\epsilon_{\gamma}(\mathbf{k})), \quad (8)$$

$$n^{(1)} = -\frac{1}{N^2 l^2} \sum_{\mathbf{k}, \mathbf{k}'} \sum_{\gamma_1, \gamma_3} \frac{1}{|\mathbf{k} - \mathbf{k}'| + q_{\text{TF}}} \times \frac{\partial f(\epsilon_{\gamma_1}(\mathbf{k}))}{\partial \epsilon_{\gamma_1}(\mathbf{k})} f(\epsilon_{\gamma_3}(\mathbf{k}')) \\ \times |\langle \gamma_3(\mathbf{k}') | \gamma_1(\mathbf{k}) \rangle|^2. \quad (9)$$

$\sum_{\alpha} |\alpha\rangle \langle \alpha| = \sum_{\gamma} |\gamma\rangle \langle \gamma|$, $f(\epsilon(\mathbf{k})) = 1/(\exp[(\epsilon(\mathbf{k}) - \mu)/T] + 1)$, and μ denotes the chemical potential. T is temperature and $k_{\text{B}} = 1$. The quantity $n^{(1)}$ is calculated as a function of $\delta\mu$ and T .

Since the number of electrons per spin and unit cell is 3, the chemical potential μ is

determined by

$$3 + n_d = n^{(0)} + g n^{(1)}, \quad (10)$$

where n_d denotes the doping concentration. For $g = 0$, $n_d = 0$, and $T=0$, μ is estimated as $\mu_0 = 1.2688$, which corresponds to $\epsilon(\mathbf{k}_D)$, i.e., the energy at the Dirac point.

We consider an external magnetic field, H_{ext} , applied in a direction parallel to the two-dimensional plane to avoid the orbital effect of the magnetic field, Noting that the Zeeman energy is given by $-\sum_j \sum_\beta \hat{m}_{j\beta} H_{\text{ext}}$, the NMR shift ($2\mu_B^2 = 1$ with μ_B being the Bohr magneton) per unit cell and at the α site is calculated as

$$\chi_\alpha = \lim_{H_{\text{ext}} \rightarrow 0} \sum_i \frac{\langle \hat{m}_{i\alpha} \rangle}{N H_{\text{ext}}} = \frac{1}{2N^2} \int_0^{1/T} \left\langle T_\tau \left(\sum_i \hat{m}_{i\alpha}(0) \sum_{j\beta} \hat{m}_{j\beta}(\tau) \right) \right\rangle_H d\tau, \quad (11)$$

where $\langle \dots \rangle_H$ denotes the average on H in Eq. (1). T_τ is the ordering operator of the imaginary time τ , $\hat{m}_{j\alpha} = \hat{n}_{j\alpha\uparrow} - \hat{n}_{j\alpha\downarrow}$, and $\hat{n}_{j\alpha\sigma} = \psi_{j\alpha\sigma}^\dagger \psi_{j\alpha\sigma}$. It is crucial that the shift at the α site is affected not only by the same kind of molecule but also by the different kinds of molecules due to four molecules per unit cell. The shift up to first order in terms of the perturbation is given by

$$\chi_\alpha \simeq \chi_\alpha^{(0)} + g \chi_\alpha^S + g \chi_\alpha^V, \quad (12)$$

which is calculated using a response function in terms of the Green function.²¹⁾ The first term denotes the zeroth order given by Fig. 3(a). The second term of Eq. (12) is the self-energy correction of the first order given by Figs. 3(b) and 3(c). The third term of Eq. (12) is the vertex correction of the first order given by Fig. 3(d). It should be noted that, in addition to the second and third terms, another contribution called the A–L term²²⁾ is generally required to satisfy the Ward identity,¹⁶⁾ as shown for the fluctuation conductivity. However Figs. 3(b), 3(c), and 3(d) are enough in the present case of the magnetic field due to the cancellation by the summation of β in $\sum_{j\beta} \hat{m}_{j\beta}(\tau)$ of Eq. (12).

The response function of the zeroth order is calculated as (Appendix C)

$$\chi_\alpha^{(0)} = \sum_\beta \chi_{\alpha\beta}^0 = -\frac{1}{N} \sum_{\mathbf{k}, \gamma} \frac{\partial f(\epsilon_\gamma(\mathbf{k}))}{\partial \epsilon_\gamma(\mathbf{k})} d_{\alpha\gamma}^*(\mathbf{k}) d_{\alpha\gamma}(\mathbf{k}), \quad (13)$$

which is rewritten as

$$\chi_\alpha^{(0)} = -\int_{-\infty}^{\infty} d\omega \frac{\partial f(\omega)}{\partial \omega} D_\alpha(\omega), \quad (14)$$

$$D_\alpha(\omega) = \frac{1}{N} \sum_{\mathbf{k}} \sum_{\gamma} \delta(\omega - \epsilon_\gamma(\mathbf{k})) d_{\alpha\gamma}^*(\mathbf{k}) d_{\alpha\gamma}(\mathbf{k}). \quad (15)$$

$D_\alpha(\omega)$ denotes the local DOS per spin and unit cell, the total DOS is $D(\omega) = \sum_\alpha D_\alpha(\omega)$, and

$\int d\omega D(\omega) = 4$. At low temperatures, for which the numerical calculation is performed in the next section, we obtain $\chi_\alpha^{(0)} \propto T$ due to $D_\alpha(\omega) \propto |\omega|$.

Performing a summation over β in Figs. 3(b) and 3(c), the second term of Eq. (12) is calculated as (Appendix C)

$$g\chi_\alpha^S = \frac{g}{2N^2l^2} \sum_{\mathbf{k}, \mathbf{k}'} \sum_{\gamma_1, \gamma_2, \gamma_3} \frac{1}{|\mathbf{k} - \mathbf{k}'| + q_{\text{TF}}} \times \frac{1}{\epsilon_2 - \epsilon_1} \left(\frac{\partial f_2}{\partial \epsilon_2} - \frac{\partial f_1}{\partial \epsilon_1} \right) \times f(\epsilon_{\gamma_3}(\mathbf{k}')) \\ \times (\langle \gamma_1(\mathbf{k}) | \alpha \rangle \langle \alpha | \gamma_2(\mathbf{k}) \rangle \langle \gamma_3(\mathbf{k}') | \gamma_1(\mathbf{k}) \rangle \langle \gamma_2(\mathbf{k}) | \gamma_3(\mathbf{k}') \rangle + (c.c.)) , \quad (16)$$

where $f_1 = f(\epsilon_1)$, $f_2 = f(\epsilon_2)$, $f_4 = f(\epsilon_4)$, $\epsilon_1 = \epsilon_{\gamma_1}(\mathbf{k})$, $\epsilon_2 = \epsilon_{\gamma_2}(\mathbf{k})$, and $\epsilon_4 = \epsilon_{\gamma_4}(\mathbf{k} - \mathbf{q})$. Performing a summation over β in Fig. 3(d), the third term of Eq. (12) is calculated as (Appendix C)

$$g\chi_\alpha^V = \frac{g}{N^2l^2} \sum_{\mathbf{k}, \mathbf{k}'} \sum_{\gamma_1, \gamma_2, \gamma_3} \frac{1}{|\mathbf{k} - \mathbf{k}'| + q_{\text{TF}}} \times \frac{f_1 - f_2}{\epsilon_1 - \epsilon_2} \times \frac{\partial f_3}{\partial \epsilon_3} \\ \times \langle \gamma_1(\mathbf{k}) | \alpha \rangle \langle \alpha | \gamma_2(\mathbf{k}) \rangle \langle \gamma_3(\mathbf{k}') | \gamma_1(\mathbf{k}) \rangle \langle \gamma_2(\mathbf{k}) | \gamma_3(\mathbf{k}') \rangle , \quad (17)$$

where $f_1 = f(\epsilon_1)$, $f_2 = f(\epsilon_2)$, $f_3 = f(\epsilon_3)$, $\epsilon_1 = \epsilon_{\gamma_1}(\mathbf{k})$, $\epsilon_2 = \epsilon_{\gamma_2}(\mathbf{k})$, and $\epsilon_3 = \epsilon_{\gamma_3}(\mathbf{k}')$.

3. NMR Shift

3.1 Chemical potential

The chemical potential $\delta\mu$ is calculated self-consistently using Eq. (10), which is rewritten as

$$n_{\text{hole}} + n_d = g n^{(1)} , \quad (18)$$

where $n_{\text{hole}} = 3 - n^{(0)}$. Equation (18) gives $\delta\mu$ as a function of T , n_d , and g , i.e., $\delta\mu(T, n_d, g)$. In order to obtain $\delta\mu$ as a function of T , n_d , and g , Eqs. (8) and (9) (i.e., $n^{(0)}$ and $n^{(1)}$) are calculated as a function of $\delta\mu$ and T , where $\delta\mu = \mu - \mu_0$ with μ_0 given by $\epsilon(\mathbf{k}_D)$ at $T = 0$.

First we examine $\delta\mu$ at $T=0$. Using the effective 2×2 Hamiltonian of the Dirac cone (Appendix A) with velocity v and tilting parameter λ , Eq. (8) is calculated as

$$n_{\text{hole}} = -\text{sgn}(\delta\mu) \frac{\delta\mu^2 l^2}{4\pi v^2} \frac{1}{(1 - \lambda^2)^{3/2}} . \quad (19)$$

In the present case of $\lambda = 0.8$ and $v/l \simeq 0.05$, $n_{\text{hole}} = -\text{sgn}(\delta\mu) C_0 \delta\mu^2$ with $C_0 \simeq 150$ (eV)⁻². Equation (9) is also estimated as $n^{(1)} = C_1 |\delta\mu|$ with $C_1 \simeq 12$ (eV)⁻² (Appendix B). Substituting these values into Eq. (18), $\delta\mu$ is obtained as follows. For $n_d = 0$, $\delta\mu = -g(C_1/C_2) (< 0)$, while $\delta\mu = (-gC_1 + \sqrt{(gC_1)^2 + 4C_0 n_d}) / (2C_0) (> 0)$ for $n_d > (gC_1)^2 / (4C_0)$. In the range of $0 < n_d < (gC_1)^2 / (4C_0)$, there are three kinds of solutions, [$\delta\mu = (-gC_1 + \sqrt{(gC_1)^2 + 4C_0 n_d}) / (2C_0)$ and $(-gC_1 \pm \sqrt{(gC_1)^2 - 4C_0 n_d}) / (2C_0)$], where we take the smallest

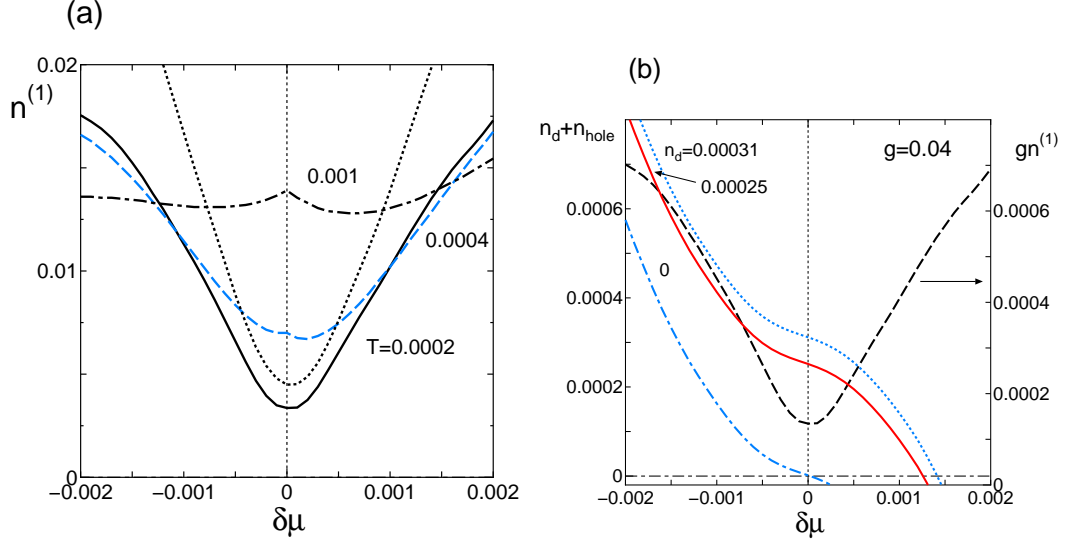


Fig. 4. (Color online) (a) $\delta\mu$ ($=\mu - \mu_0$) dependence of $n^{(1)}$ with fixed $T = 0.001, 0.0004,$ and 0.0002 , where the dotted line denotes $n^{(1)}$ with $q_{TF} = 0$ at $T=0.0002$. (b) $\delta\mu$ dependence of $n_{\text{hole}} + n_d$ and $gn^{(1)}$ for $T = 0.0002$ with $g=0.04$, where $n_{\text{hole}} = 3 - n^{(0)}$ and n_d denotes the doping concentration. $\mu_0 (= 1.2688)$ denotes the chemical potential for $T = 0$ and $n_d = 0$ in the absence of interaction. The intersection gives a solution for $\delta\mu$, where the lowest one is taken when there are many solutions.

one, $\delta\mu = (-gC_1 - \sqrt{(gC_1)^2 - 4C_0n_d})/(2C_0) (< 0)$, in order to obtain a solution connected continuously to that of $T=0$. Thus, a first-order transition occurs at $n_d = (gC_1)^2/(4C_0)$, where the sign of the chemical potential $\delta\mu$ changes from negative to positive with decreasing g or increasing n_d .

Here we mention the state given by $\delta\mu < 0$ for $n_d = 0$. Since $\delta\mu < 0$ gives $n^{(1)} > 0$ from Eqs. (9) and (B-4), the chemical potential is located at the valence band with $\epsilon_2(\mathbf{k}) - \mu_0 = \delta\mu (< 0)$. This implies the emergence of an excess electron density at \mathbf{k} with $\epsilon_2(\mathbf{k}) = \mu$ in the valence band, which has the effect of reducing the chemical potential to keep the total number of filled electrons. Thus, holes exist in the valence band below the Dirac point (i.e., the valley of the Dirac cone) even for $n_d = 0$.

Next we examine $\delta\mu$ for $T \neq 0$, which is calculated numerically from Eq. (10). When there is more than one solution, we choose the smallest one in order to be consistent with that of $T = 0$. Figure 4(a) shows the $\delta\mu$ dependence of $n^{(1)}$ for fixed $T = 0.0002$ (solid line), 0.0004 (dashed line) and 0.001 (dot-dashed line). The quantity $n^{(1)}$ is positive, where $n^{(1)} = 0$ at $T=0$, and $n^{(1)}$ at low temperatures is proportional to T due to the factor $-\partial f(\epsilon_{\gamma_1}(\mathbf{k}))/\partial \epsilon_{\gamma_1}(\mathbf{k})$. It is found that $n^{(1)}$ as a function of $\delta\mu$ shows $n^{(1)}(\delta\mu) - n^{(1)}(0) \propto \delta\mu^2$ for small $\delta\mu$, although there is a slight deviation from the symmetric behavior and a slight maximum at $\delta\mu = 0$. In order

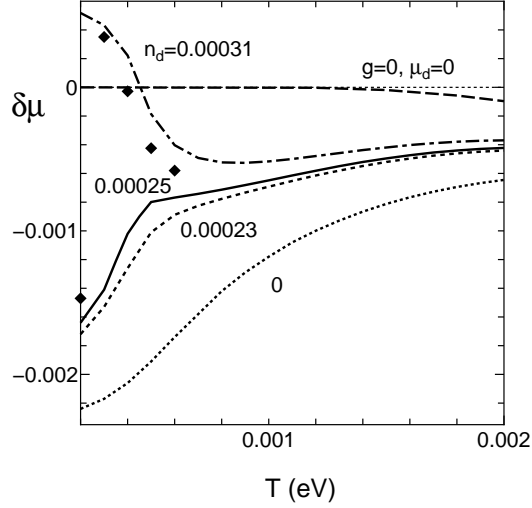


Fig. 5. T dependence of $\delta\mu$ for $g = 0.04$ with fixed $n_d = 0.00031, 0.00025, 0.00023,$ and 0 , which are obtained from $n_d + n_{\text{hole}} = gn^{(1)}$. The symbols (diamonds) correspond to $\delta\mu$ for $n_d = 0.00028$. The dashed line ($g=0$) denotes $\delta\mu$ for $g = 0$ and $n_d = 0$.

to see the suppression of $n^{(1)}(\delta\mu)$ by the screening, $n^{(1)}$ with $q_{TF} = 0$ at $T=0.0002$ (dotted line) is compared with the solid line. Figure 4(b) shows the $\delta\mu$ dependence of $n_d + n_{\text{hole}}$ and $gn^{(1)}$ with $g = 0.04$ for $T=0.0002$, where the intersection gives a solution of $\delta\mu$. Thus, the chemical potential $\delta\mu$ is calculated self-consistently for fixed T , n_d , and g . The solution of $\delta\mu$ is a single value for $n_d = 0.00031$ and 0 . For $n_d=0.00025$, there are three solutions and the lowest $\delta\mu$ is chosen as shown for $T=0$.

Figure 5 shows the T dependence of $\delta\mu$ with some choices of n_d for $g=0.04$, where there are the following three types of T dependence of $\delta\mu$, depending on n_d . For large n_d ($= 0.00031$), there is a crossover from $\delta\mu > 0$ to $\delta\mu < 0$ with increasing T (> 0.0001). $\delta\mu$ takes a minimum above the temperature corresponding to $\delta\mu = 0$. For small n_d ($=0.00023$ and 0), $\delta\mu < 0$ exists for arbitrary T and $\delta\mu$ increases monotonically with increasing T . In the region of $0.0026 < n_d < 0.00031$ (for example, $n_d = 0.0028$ (diamonds)), $\delta\mu$ jumps from $\delta\mu < 0$ to $\delta\mu > 0$ with increasing T (> 0.0002), while such a jump diminishes for $T > 0.005$. Based on more precise calculation, we find that the jump of $\delta\mu$ occurs at $(n_d, T) \simeq (0.00032, 0), (0.00031, 0.0002), (0.00028, 0.0003), (0.00026, 0.0004)$, forming a line of the boundary between $\delta\mu < 0$ and $\delta\mu > 0$, which terminates before $T \simeq 0.0005$. For simplicity, the present paper does not treat such a region where a first-order transition occurs at low temperatures ($T < 0.0005$). Using $\delta\mu$ of Fig. 5 with a moderate choice of n_d , we examine the NMR shift χ_α in the next section to obtain a similar result to that of an experiment at low temperatures. The choice of n_d is discussed in Sect. 4.

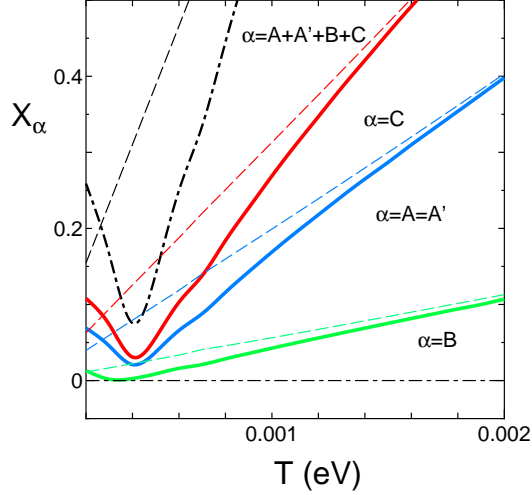


Fig. 6. (Color online) T dependence of NMR shift χ_α with $\alpha = A (=A')$, B, and C for $g = 0.04$ and $n_d = 0.00025$. The dashed line denotes $\chi_\alpha^{(0)}$ for $g = 0$, $n_d = 0.0$, and $\delta\mu = 0$. Note that $\chi - \chi^{(0)}$ corresponds to the sum of the self-energy and vertex corrections, where $\chi = \chi_{A+A'+B+C}$.

3.2 NMR shift

The numerical calculation of the NMR shift is performed as follows. The zeroth-order term given by Eq. (13) is calculated by dividing the summation into $n = 200$ segments for the axes of k_x and k_y in the first Brillouin zone. Equation (7a) is calculated in the reduced region consisting of two valleys around the Dirac point $\pm\mathbf{k}_D$. In order to examine the effect of the interaction at low temperatures of $T < 0.002$, the calculation of Eqs. (9), (16), and (17) is performed by choosing $|\mathbf{k} \pm \mathbf{k}_D|/\pi < 0.1$ with 40 segments. This choice is reasonable since the change by $|\mathbf{k} \pm \mathbf{k}_D|/\pi < 0.14$ is less than 10%. The NMR shift is examined in the range of $0.0002 < T < 0.002$ due to the limited number of segments.

Using the chemical potential $\delta\mu$ obtained in Fig. 5, we calculate Eq. (12) to examine the T dependence of the NMR shift. Figure 6 shows the T dependence of χ_α with $g = 0.04$ and $n_d = 0.00025$, where $\alpha = A(=A')$, B, and C denotes the shift for the respective site and $\alpha = A+A'+B+C$ denotes the sum of the shift. It is noticed that the relation $\chi_C > \chi_A > \chi_B$ still holds even in the presence of the interaction. The dashed line denotes $\chi_\alpha^{(0)}$, i.e., the shift in the case of $g = 0$, which is proportional to T .¹⁰⁾ Compared with $\chi_\alpha^{(0)}$, χ_α exhibits a noticeable reduction, i.e., suppression, which comes from $g(\chi^S + \chi^V)$ (< 0). At $T \simeq 0.0005$, χ_C and χ_A show a minimum and $\chi_C \simeq \chi_A$, while χ_B reduces almost to zero. There is an enhancement of χ_C and χ_A at low temperatures due to the finite $|\delta\mu|$, which increases $\chi_\alpha^{(0)}$. The suppression of χ_α becomes large for larger g since $g\chi^S$ and $g\chi^V$ are mainly proportional to g .

In order to understand the suppression of χ_α , the contributions of self-energy and vertex

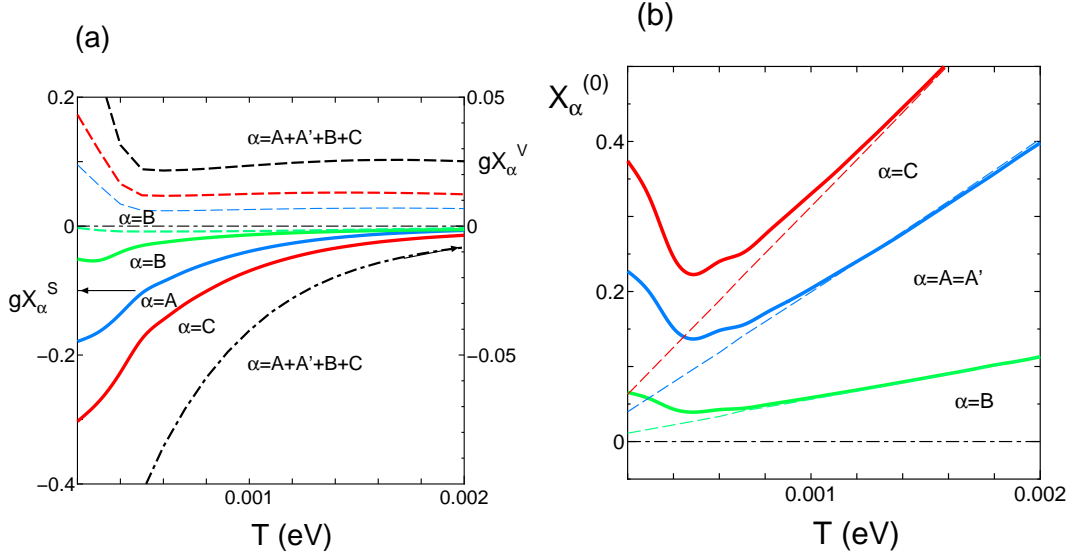


Fig. 7. (Color online) (a) T dependence of the self-energy (solid line) and vertex corrections (dashed line) corresponding to Fig. 6. (b) T dependence of the corresponding $\chi_\alpha^{(0)}$ with $\mu \neq 0$ and $g=0.4$. For $0.0004 < T$, $g\chi_\alpha^S (< 0)$ takes a larger magnitude than that of $g\chi_\alpha^V (> 0)$. Thus, the self-energy correction determines the suppression of χ_α in Fig. 6.

corrections are examined in Fig. 7(a). The effect of the self-energy correction $g\chi^S$ is much larger than that of the vertex correction $g\chi^V$ at low temperatures of $T < 0.0015$. For $0.0015 < T < 0.002$, the contribution of $g\chi^V (> 0)$ becomes comparable with that of $g\chi^S (< 0)$, and then the suppression of χ_α becomes small. At higher temperatures, it is expected that the vertex correction becomes dominant compared with the self-energy correction, i.e., χ_α is enhanced compared with $\chi_\alpha^{(0)}$. Figure 7(b) shows $\chi_\alpha^{(0)} (= \chi_\alpha - g\chi_\alpha^S - g\chi_\alpha^V)$, which is always larger than χ_α in the absence of the interaction (dashed line) due to $\delta\mu \neq 0$. At low temperatures, $\chi_\alpha^{(0)}$ is enhanced due to the increase in $|\delta\mu|$.

We examine χ_α for some other values of n_d for comparison with Fig. 6. Figure 8(a) shows χ_α for $n_d = 0.00031$, where the T dependence of χ_α is similar but the height is slightly larger than that for $n_d = 0.00025$. The case of $n_d = 0.00031$, where $\delta\mu (> 0)$ for $T < 0.0004$, is almost on the boundary of the jump in μ . χ_α for $n_d = 0.00028$ is similar but a jump below the minimum occurs at higher temperatures. Figure 8(b) shows χ_α for $n_d = 0.00023$. The T dependence of χ_α is similar to that of $n_d = 0.00025$ but the height is also large. For $n_d = 0.00023$, $\delta\mu (< 0)$ is slightly lower than that of $n_d = 0.00025$ owing to being away from the boundary of the jump of $\delta\mu$. Thus, there is an optimum value of n_d that gives the lowest χ_α . Such n_d is lower and moderately away from the boundary of the jump. The case of $n_d = 0$ is shown in Fig. 8(c) to understand the role of n_d by comparison with Fig. 6. The height of

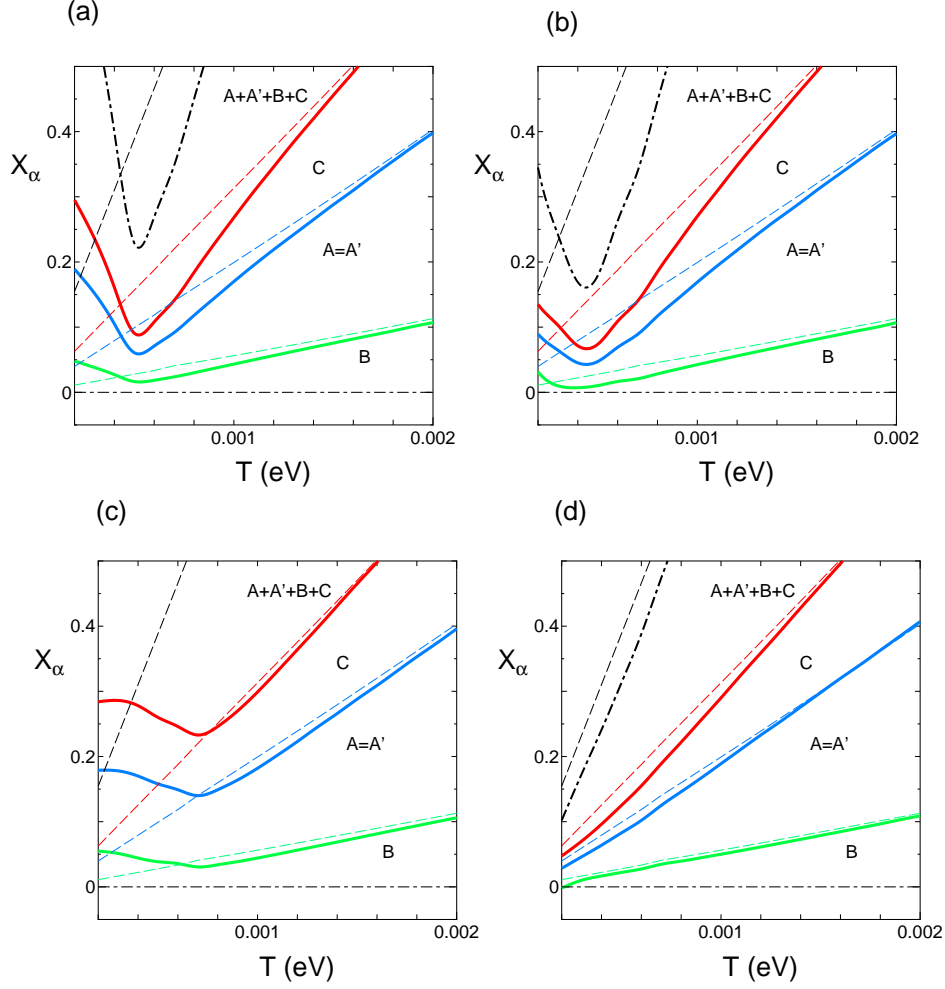


Fig. 8. (Color online) T dependence of χ_α with $g=0.04$ for $n_d = 0.00031$ (a), $n_d = 0.00023$ (b), $n_d = 0$ (c), and $\mu = 0$ (d). Notations are the same as in Fig. 6. $\delta\mu$ in (c) is determined self-consistently. For $0.0008 < T$, $\delta\chi_\alpha (= \chi_\alpha - \chi_\alpha^{(0)})$ is negative but small due to the competition of $g\chi_\alpha^S$ and $\chi_\alpha^{(0)}$. For $n_d = 0$, $\delta\mu$ becomes much lower than that of Fig. 4. Thus, the deviation of $\delta\mu$ from zero gives the enhancement of the DOS. This enhances the magnitude of both $g\chi_\alpha^S$ and $\chi_\alpha^{(0)}$. (d) T dependence of $\delta\chi_\alpha$, which is similar to that in (c), but χ_α^S is much smaller due to the small DOS. The enhancement of $\delta\chi_\alpha$ at low temperatures is absent due to $\mu = 0$.

χ_α further increases, but a small suppression ($\chi_\alpha - \chi_\alpha^{(0)} < 0$) for $0.0008 < T$ still exists due to competition between the enhancement of $\chi_\alpha^{(0)}$ and the decrease in $g\chi_\alpha^S$, which occurs for large $|\delta\mu|$. However a large enhancement of χ_α is seen at low temperatures since the effect of $|\delta\mu| \neq 0$ on $\chi_\alpha^{(0)}$ is larger than that of $|g\chi_\alpha^S|$ at low temperatures. Thus, it turns out that n_d with a moderate magnitude has the effect of reducing χ_α . Figure 8(d) shows χ_α for $\delta\mu = 0$ and $g = 0.04$. Although the interaction gives $\delta\mu \neq 0$, the case of $\delta\mu = 0$ is compared with Fig. 6 to clarify the role of $\delta\mu$ in χ_α . For $\delta\mu = 0$, the reduction given by $\chi_\alpha - \chi_\alpha^{(0)} < 0$ still exists

but is small. A minimum of χ_α is absent and χ_α decreases monotonically. The magnitudes of χ^S and χ^V are smaller but their T dependence is similar to that in Fig. 7(a) except for low $T (< 0.0005)$.

Thus, the origin of the minimum of χ_α is as follows. When $|\delta\mu|$ increases from zero (as found by the presence of $g \neq 0$), the DOS at the chemical potential increases, and the increase in $|\chi^S|$ becomes much larger than χ^V , resulting in the large suppression of χ_α , as seen from Fig. 6. However, $|\delta\mu|$ also increases $\chi_\alpha^{(0)}$ at $T < 0.0006$ as shown in Fig. 7. Such competition gives a minimum of χ_α at $T \simeq 0.0004$ in Fig. 6.

4. Summary and discussion

We examined the NMR shift χ_α at low temperatures of $T < 0.002$ eV for massless Dirac electrons in the organic conductor α -(BEDT-TTF)₂I₃. The response function was calculated in the presence of the long-range Coulomb interaction, where screenings were taken into account. Treating the interaction up to the first order in the perturbation, the chemical potential in the presence of the doping n_d was calculated self-consistently, and the response function was calculated for both self-energy and vertex corrections to satisfy the Ward identity. The self-consistent solution of $\delta\mu$ was examined on the plane of n_d and T . The suppression of χ_α was obtained using n_d close to the boundary between $\delta\mu > 0$ and $\delta\mu < 0$ at $T = 0$. We found a novel fact that both $\chi_B^S < 0$ and $\chi_B^V < 0$. The suppression of χ_α originates from the self-energy correction being dominant over the vertex correction. A minimum of χ_α exists at low temperatures. At lower temperatures, the shift is enhanced due to $\delta\mu \neq 0$.

Here we compare Fig. 6 with other previous work. The fact that the sign of the vertex correction $\chi_\alpha^{(V)}$ is positive for $\alpha = A$ and C but negative for B is compatible with the model with the on site-repulsive interaction.¹⁸⁾ This suggests a common feature of the vertex correction even though the interaction range is different between these models. The fact that $0 > g\chi_{A+A'+B+C}^S$ at low temperatures is consistent with the sign expected by the calculation of the self-energy of the Green function.¹⁴⁾ The negative sign of $\chi_{A+A'+B+C}^{(S)}$ in the present paper is the same as that obtained by calculating the renormalization of the velocity of the Dirac cone in terms of such a Green function.¹⁵⁾ In the present calculation, a large suppression of χ_α is obtained for a finite doping (n_d) with $\delta\mu \neq 0$, while suppression is obtained in the absence of doping with $\delta\mu = 0$ for the case of velocity renormalization.

We note a reduced model of a 2×2 Hamiltonian²³⁾ consisting of only two bands, the conduction and valence bands, which are obtained from $\epsilon_1(\mathbf{k})$ and $\epsilon_2(\mathbf{k})$ with $d_{\alpha,1}$ ($\alpha = A (= A')$, B , C) in Eqs. (6a) and (6b). Calculating Eqs. (9), (16), and (17) with these two bands

and all the α , we found that the difference in the numerical result between the reduced model and the 4×4 Hamiltonian (Eq. (5)) is about 3% suggesting the validity of the effective 2×2 Hamiltonian with a choice of the base in terms of the Luttinger–Kohn representation.²³⁾ The present calculation gives the NMR shift directly owing to the diagonalization of Eq. (5) for each \mathbf{k} . Although the comparison of the intermediate process with the effective Hamiltonian is complicated due to the factors $d_{\alpha,1}$ and $d_{\alpha,2}$ depending on the choice of the base, the same result of the NMR shift is expected when the components of the base are reasonably taken into account.

We took n_d as a parameter to explain the NMR shift. The parameter is located slightly away from the first-order transition since, at present, such a transition has not been found experimentally. The existence of $n_d (> 0)$ is claimed from the Hall conductivity, where a theory without interaction²⁴⁾ predicted $n_d \simeq 10^{-6}$ and an experiment²⁵⁾ estimated $n_d = (0.1 - 1) \times 10^{-5}$. The experimental estimation is reasonable owing to the enhancement of n_d by the interaction. However, the present choice of $n_d \simeq 10^{-4}$, which is larger than the experimental value, still remains a problem to be resolved in the future.

Finally we discuss the relevance of the present work to the experiment on the NMR shift in α -(BEDT-TTF)₂I₃. Site-selective NMR shows that the electron susceptibility decreases with decreasing T below < 0.01 eV with $\chi_C > \chi_A (= \chi_{A'}) > \chi_B$,^{11,12)} where the suppression from the T linear dependence of χ_α is visible and the strong suppression of χ_B shows a gaplike T dependence. The behavior at lower temperatures is as follows.¹³⁾ For $T < 0.005$, χ_B becomes almost zero with a minimum. Also both χ_A and χ_C decrease rapidly. At $T \simeq 0.002$, all χ_α become almost zero. This experimental result is compared with our theoretical result of χ_α in Fig. 6 ($n_d = 0.00025$ and $g = 0.04$), which shows a large suppression of χ_B at low temperatures. Thus, a common T dependence is seen for temperatures above the minimum. However, the present calculation shows an enhancement at lower temperatures while the experiment shows monotonic decreases in χ_C and χ_A . Further, the characteristic temperature in the present calculation is much lower than that in the experiment. Such a difference may be reduced by considering a larger magnitude of g . Another comment is regarding the chemical potential $\delta\mu$ as shown in Fig. 5. For larger $n_d (= 0.0003)$, the T dependence of $\delta\mu$, which moves from positive to negative, is qualitatively similar to that obtained theoretically in terms of carrier doping without interaction.²⁴⁾ In fact, such a change of the sign, which gives rise to the change in the Hall coefficient, was verified by an experiment on the Hall conductivity.²⁵⁾

Acknowledgements

The author thanks H. Fukuyama for the suggestion of the problem and valuable comments, and A. Kobayashi for useful discussions. This work was supported by JSPS KAKENHI Grant Numbers JP15H02108 and JP26400355.

Appendix A: Effective interaction

We analytically calculate the screening constant for the bare Coulomb interaction (Eq. (3)) using an effective 2×2 Hamiltonian^{23,24)} for the Dirac cone around the Dirac point \mathbf{k}_D , given by

$$H_{\text{eff}} = \begin{pmatrix} v\tilde{k}_y + \lambda v\tilde{k}_x & v\tilde{k}_x \\ v\tilde{k}_x & -v\tilde{k}_y + \lambda v\tilde{k}_x \end{pmatrix}, \quad (\text{A}\cdot 1)$$

where $\tilde{\mathbf{k}} = (\tilde{k}_x, \tilde{k}_y) = \mathbf{k} - \mathbf{k}_D$ with the Dirac point \mathbf{k}_D . For simplicity we rewrite as $\tilde{\mathbf{k}} \rightarrow \mathbf{k}$. The eigenvalue of Eq. (A.1) is given by $\xi_{\gamma, \mathbf{k}} = v\lambda k_x + \gamma v|\mathbf{k}|$ with $(\gamma = \pm)$. Equation (A.1) describes the Dirac cone with tilting parameter λ , where the k_x axis is taken as the tilting direction. The polarization function of Eq. (A.1), which is given by the density-density response function, is written as²⁶⁾

$$\Pi(\mathbf{q}, \delta\mu, T) = -\frac{2}{N^2} \sum_{\gamma, \gamma'} \sum_{\mathbf{k}} \frac{1 + \gamma\gamma'(\mathbf{k} \cdot \mathbf{k}')/|\mathbf{k}||\mathbf{k}'|}{2} \times \frac{f(\xi_{\gamma, \mathbf{k}}) - f(\xi_{\gamma', \mathbf{k}'})}{-\xi_{\gamma', \mathbf{k}'} + \xi_{\gamma, \mathbf{k}}}, \quad (\text{A}\cdot 2)$$

where $\mathbf{k}' = \mathbf{k} + \mathbf{q}$ and $f(\xi) = 1/(\exp[(\xi - \delta\mu)/T] + 1)$. Using Eq. (A.2), the effective Coulomb interaction within the RPA is written as

$$v_{\mathbf{q}, \text{eff}} = \frac{v_{\mathbf{q}}}{1 + q_{\text{TF}}/q} = \frac{gl}{|\mathbf{q}| + q_{\text{TF}}}, \quad (\text{A}\cdot 3)$$

where

$$v_{\mathbf{q}} = \frac{v_q^0/\epsilon_2}{1 + v_q^0\Pi(\mathbf{q}, 0, 0)} = \frac{v_q^0}{\epsilon} \equiv \frac{gl}{q}, \quad (\text{A}\cdot 4)$$

$$\Pi(\mathbf{q}, 0, 0) = \frac{q}{2\pi v} \left\langle \frac{1}{\sqrt{1 - \lambda^2 \cos^2 \theta_q}} \right\rangle_{\theta_q}, \quad (\text{A}\cdot 5)$$

$g = 2\pi e^2/(\epsilon l)$, $v_q^0 = 2\pi e^2/q$, $q = |\mathbf{q}|$, and l is the lattice constant. $\epsilon = \epsilon_1\epsilon_2$. $\epsilon_1 (= 1 + v_q^0\Pi(\mathbf{q}, 0, 0))$ ²⁶⁾ is the intralayer dielectric constant and ϵ_2 denotes the interlayer dielectric constant, taken as $\simeq 5$. $\langle \rangle_{\theta}$ denotes the average over the angle $\theta = \theta_q$, which denotes the angle between \mathbf{q} and the tilted axis of the Dirac cone with tilting parameter λ . Equation (A.5) is multiplied by 4 due to the freedom of the spin and valley. In Eq. (A.3), the denominator, $1 + q_{\text{TF}}/q$, is an interpolation formula used to describe the crossover between small $q (\ll q_{\text{TF}})$ and large $q (\gg q_{\text{TF}})$. This gives a reasonable result compared with the exact one.²⁶⁾ Assuming only the intralayer screening due to $\delta\mu (\neq 0)$, q_{TF} is written as

$$q_{\text{TF}} = qv_{\mathbf{q}}\Pi(0, \delta\mu, T) \simeq qv_{\mathbf{q}} \times \frac{4(|\delta\mu| + T)}{2\pi v^2(1 - \lambda^2)^{3/2}}, \quad (\text{A}\cdot 6)$$

which is the Thomas–Fermi screening including temperature. Thus, q_{TF} is estimated as

$$q_{\text{TF}} \simeq \frac{4e^2/v}{\epsilon(1 - \lambda^2)^{3/2}} \times \frac{|\delta\mu| + T}{v} \simeq 2.5 \times \frac{|\delta\mu| + T}{v}, \quad (\text{A}\cdot 7)$$

where $g = 0.21/\epsilon_2$, $\epsilon_1 = 1 + v_q^0 \Pi(\mathbf{q}, 0, 0) \simeq 40$. In deriving Eq. (A·7), we used the parameters $\lambda \simeq 0.8$, $e^2/v = 27.2$, $2\pi e^2/l = 8.5$ eV, $v/l = 0.05$ eV, $\langle (1 - \lambda^2 \cos^2 \theta)^{-1/2} \rangle_{\theta} = 1.43$, and $(1 - \lambda^2)^{-3/2} = 4.62$. Note that $g = 0.04$ corresponds to $\epsilon_2 \simeq 5$.

Appendix B: Number density

Using the matrix, $S(1/T) = T_\tau \exp[-\int_0^{1/T} H_{\text{int}}(\tau) d\tau]$,²¹⁾ where T_τ is the ordering operator of the imaginary time (τ) and $H_{\text{int}}(\tau) = e^{(H_0 - \mu)\tau} H_{\text{int}} e^{-(H_0 - \mu)\tau}$, we calculate the density and response functions up to the first order in H_{int} .

The number density per unit cell and per spin is calculated from

$$\lim_{\tau \rightarrow -0} \frac{1}{N} \sum_i \sum_\alpha \frac{-\langle T_\tau (\psi_{i,\alpha}(\tau) \psi_{i,\alpha}(0)^\dagger S(1/T)) \rangle_0}{\langle S(1/T) \rangle_0} \simeq n^{(0)} + gn^{(1)}, \quad (\text{B}\cdot 1)$$

where $\langle \rangle_0$ denotes the thermal average on H_0 . From Eq. (6a) with $\psi_{\mathbf{k}\alpha} = \sum_\gamma d_{\alpha\gamma}(\mathbf{k}) \psi_{\mathbf{k}\gamma}$, the density of the zeroth order shown in Fig. 2(a) is calculated as

$$\begin{aligned} n^{(0)} &= \frac{1}{N} \sum_i \sum_\alpha \langle \psi_{i,\alpha}^\dagger \psi_{i,\alpha} \rangle_0 = \frac{1}{N} \sum_{\mathbf{k}} \sum_\alpha \langle \psi_{\mathbf{k}\alpha}^\dagger \psi_{\mathbf{k}\alpha} \rangle_0 \\ &= \frac{1}{N} \sum_\gamma \sum_{\mathbf{k}} \sum_\alpha d_{\alpha\gamma}(\mathbf{k})^* d_{\alpha\gamma}(\mathbf{k}) \times \langle \psi_{\mathbf{k}\gamma}^\dagger \psi_{\mathbf{k}\gamma} \rangle_0 \\ &= \frac{1}{N} \sum_\gamma \sum_{\mathbf{k}} T \sum_n G(n, \epsilon_\gamma(\mathbf{k})) = \frac{1}{N} \sum_\gamma \sum_{\mathbf{k}} f(\epsilon_\gamma(\mathbf{k})). \end{aligned} \quad (\text{B}\cdot 2)$$

The Green function is given by $G(n, \epsilon_\gamma(\mathbf{k})) = \int (-T_\tau \langle \psi_{\mathbf{k}\gamma}(\tau) \psi_{\mathbf{k}\gamma}(0)^\dagger \rangle e^{-i\omega_n \tau} d\tau = (i\omega_n + \mu - \epsilon_\gamma(\mathbf{k}))^{-1}$, where $\omega_n (= (2n + 1)\pi T)$ is the Matsubara frequency with n being an integer and $T \sum_n G(n, \epsilon_\gamma(\mathbf{k})) = f(\epsilon_\gamma(\mathbf{k})) = 1/(\exp[(\epsilon_\gamma(\mathbf{k}) - \mu)/T] + 1)$.

The density of the first order is calculated as (Fig. 2(b))

$$\begin{aligned} gn^{(1)} &= -g \frac{T^2}{N^2 l^2} \sum_{n,n'} \sum_{\mathbf{k}, \mathbf{q}} \sum_{\gamma_1, \gamma_2, \gamma_3} \sum_{\alpha', \beta'} \frac{1}{|\mathbf{q}| + q_{\text{TF}}} G(n, \epsilon_{\gamma_1}(\mathbf{k})) G(n, \epsilon_{\gamma_2}(\mathbf{k})) G(n', \epsilon_{\gamma_3}(\mathbf{k} - \mathbf{q})) \\ &\quad \times d_{\alpha'\gamma_1}^*(\mathbf{k}) d_{\alpha'\gamma_1}(\mathbf{k}) d_{\alpha'\gamma_3}^*(\mathbf{k} - \mathbf{q}) d_{\beta'\gamma_3}(\mathbf{k} - \mathbf{q}) d_{\beta'\gamma_2}^*(\mathbf{k}) d_{\alpha\gamma_2}(\mathbf{k}) \\ &= -g \frac{T^2}{N^2 l^2} \sum_{n,n'} \sum_{\mathbf{k}, \mathbf{q}} \sum_{\gamma_1, \gamma_3} \sum_{\alpha', \beta'} \frac{1}{|\mathbf{q}| + q_{\text{TF}}} G(n, \epsilon_{\gamma_1}(\mathbf{k}))^2 G(n', \epsilon_{\gamma_3}(\mathbf{k} - \mathbf{q})) \\ &\quad \times d_{\alpha'\gamma_1}(\mathbf{k}) d_{\beta'\gamma_1}^*(\mathbf{k}) d_{\alpha'\gamma_3}^*(\mathbf{k} - \mathbf{q}) d_{\beta'\gamma_3}(\mathbf{k} - \mathbf{q}) \\ &= -g \frac{1}{N^2 l^2} \sum_{\mathbf{k}, \mathbf{q}} \sum_{\gamma_1, \gamma_3} \sum_{\alpha', \beta'} \frac{1}{|\mathbf{q}| + q_{\text{TF}}} \times \frac{\partial f(\epsilon_{\gamma_1}(\mathbf{k}))}{\partial \epsilon_{\gamma_1}(\mathbf{k})} \times f(\epsilon_{\gamma_3}(\mathbf{k} - \mathbf{q})) \\ &\quad \times d_{\alpha'\gamma_1}(\mathbf{k}) d_{\beta'\gamma_1}^*(\mathbf{k}) d_{\alpha'\gamma_3}^*(\mathbf{k} - \mathbf{q}) d_{\beta'\gamma_3}(\mathbf{k} - \mathbf{q}). \end{aligned} \quad (\text{B}\cdot 3)$$

Equation (B·3) leads to Eq. (9). Note that $gn^{(1)} > 0$ since $-\partial f(\epsilon)/\partial \epsilon > 0$ and $f(\epsilon) > 0$.

At $T=0$, Eq. (9) is examined using an effective 2×2 Hamiltonian (Appendix A) with $\gamma = \pm$ and tilting parameter λ , where the Dirac cone is tilted with maximum velocity $v(1 + \lambda)$ and

minimum velocity $v(1 - \lambda)$. Equation (9) is calculated as

$$n^{(1)} = \frac{|\delta\mu|l^3}{2\pi^2} \int_0^{k_c} dy y \sum_{\gamma_3=\pm} \left\langle \frac{f(\epsilon_{\gamma_3}(\mathbf{k}')) < \gamma_3(\mathbf{k}') | \gamma_1(\mathbf{k}) > |^2 / v(\theta)^2}{\sqrt{k_\mu^2 + y^2 - 2yk_\mu \cos(\theta - \theta') + q_{\text{TF}}(\delta\mu, 0)}} \right\rangle_{\theta, \theta'}, \quad (\text{B}\cdot\text{4})$$

where $\delta\mu = \mu - \mu_0$ with μ_0 given by $\epsilon(\mathbf{k}_D)$ at $T = 0$. $\gamma_1 = +$ or $-$, $\langle \rangle_\theta$ denotes an average with respect to θ , $y = k'$, $k_c (>> \delta\mu/v)$ is the momentum cutoff of the Dirac cone $v_\theta = v(1 + \lambda \cos \theta)$, $\mathbf{k} = k(\cos \theta, \sin \theta)$, $\mathbf{k}' = k'(\cos \theta', \sin \theta')$, and $k_\mu = |\delta\mu|/v(\theta)$. For $\lambda = 0.8$ and $v/l \simeq 0.05$, the numerical estimation gives $n^{(1)} = C_1 |\delta\mu|$ with $C_1 \simeq 12 \text{ (eV)}^{-2}$.

Appendix C: Response function

The NMR shift at the α site is obtained from

$$\chi_\alpha = \sum_\beta \chi_{\alpha\beta} \simeq \chi_\alpha^{(0)} + g\chi_\alpha^S + g\chi_\alpha^V, \quad (\text{C}\cdot\text{1})$$

where $\chi_{\alpha\beta}$ is the response function between the α and β sites, which is calculated by²¹⁾

$$\chi_{\alpha\beta} = \frac{1}{N} \sum_{\mathbf{k}} \int_0^{1/T} \frac{\langle T_\tau (\psi_{\mathbf{k}\alpha}^\dagger(\tau) \psi_{\mathbf{k}\alpha}(\tau) \psi_{\mathbf{k}\beta}^\dagger(0) \psi_{\mathbf{k}\beta}(0) S(1/T)) \rangle_0}{\langle S(1/T) \rangle_0} e^{i\omega_n \tau} d\tau |_{i\omega_n \rightarrow +i0} \quad (\text{C}\cdot\text{2})$$

We took $2\mu_B^2$ as unity with μ_B being the Bohr magneton. Equation (C-2) is calculated by expanding $S(1/T)$, in terms of H_{int} where the zeroth order gives $\chi_\alpha^{(0)}$ and the first order gives $g\chi_\alpha^S + g\chi_\alpha^V$. In the second-order terms, there is the A-L contribution whose diagram reduces to a disconnected diagram²¹⁾ in the absence of H_{int} . Such a contribution, which is added to Eq. (C-1) to satisfy the Ward identity¹⁶⁾ for the RPA given by Eq. (7b), vanishes in the present case due to the summation of $\hat{m}_{j\beta}$ in Eq. (11) with respect to β .

From Fig. 3(a), the zeroth order is calculated as

$$\begin{aligned} \chi_\alpha^{(0)} &= -\frac{T}{N} \sum_n \sum_{\mathbf{k}} \sum_{\gamma, \gamma'} \sum_\beta G(n, \epsilon_\gamma(\mathbf{k})) G(n, \epsilon_{\gamma'}(\mathbf{k})) d_{\alpha\gamma}^*(\mathbf{k}) d_{\beta\gamma}(\mathbf{k}) d_{\beta\gamma'}^*(\mathbf{k}) d_{\alpha\gamma'}(\mathbf{k}) \\ &= -\frac{1}{N} \sum_{\mathbf{k}} \sum_{\gamma, \gamma'} \sum_\beta \frac{f(\epsilon_\gamma(\mathbf{k})) - f(\epsilon_{\gamma'}(\mathbf{k}))}{\epsilon_\gamma(\mathbf{k}) - \epsilon_{\gamma'}(\mathbf{k})} d_{\alpha\gamma}^*(\mathbf{k}) d_{\beta\gamma}(\mathbf{k}) d_{\beta\gamma'}^*(\mathbf{k}) d_{\alpha\gamma'}(\mathbf{k}) \\ &= -\frac{1}{N} \sum_{\mathbf{k}, \gamma} \frac{\partial f(\epsilon_\gamma(\mathbf{k}))}{\partial \epsilon_\gamma(\mathbf{k})} d_{\alpha\gamma}^*(\mathbf{k}) d_{\alpha\gamma}(\mathbf{k}). \end{aligned} \quad (\text{C}\cdot\text{3})$$

In Eq. (C-3), we used the identity

$$\sum_\beta d_{\beta\gamma}(\mathbf{k}) d_{\beta\gamma'}^*(\mathbf{k}) = \delta_{\gamma, \gamma'}, \quad (\text{C}\cdot\text{4})$$

which is also applied in the following calculation of $g\chi_\alpha^S$ and $g\chi_\alpha^V$.

The first order consists of the self-energy correction $g\chi_\alpha^S$ and the vertex correction $g\chi_\alpha^V$.

From Figs. 3(b) and 3(c), the self-energy correction is calculated as

$$g\chi_\alpha^S = \frac{gT^2}{N^2l^2} \sum_{n,n'} \sum_{\mathbf{k},\mathbf{q}} \frac{1}{|\mathbf{q}| + q_{\text{TF}}} \sum_{\gamma_1,\gamma_2,\gamma_3,\gamma_4} \sum_{\alpha',\beta'} \sum_{\beta} G(n, \epsilon_{\gamma_1}(\mathbf{k})) G(n', \epsilon_{\gamma_4}(\mathbf{k} - \mathbf{q})) G(n, \epsilon_{\gamma_3}(\mathbf{k})) G(n, \epsilon_{\gamma_2}(\mathbf{k})) \\ \times d_{\alpha\gamma_1}^*(\mathbf{k}) d_{\alpha'\gamma_1}(\mathbf{k}) d_{\alpha'\gamma_4}^*(\mathbf{k} - \mathbf{q}) d_{\beta'\gamma_4}(\mathbf{k} - \mathbf{q}) d_{\beta'\gamma_3}^*(\mathbf{k}) d_{\beta\gamma_3}(\mathbf{k}) d_{\beta'\gamma_2}^*(\mathbf{k}) d_{\alpha\gamma_2}(\mathbf{k}) + (1 \leftrightarrow 2). \quad (\text{C}\cdot 5)$$

Using Eq. (C.4) and the partial fraction decomposition in terms of $G(n, \epsilon_\gamma)$,

$$g\chi_\alpha^S = \frac{g}{N^2l^2} \lim_{3 \rightarrow 2} \sum_{\mathbf{k},\mathbf{q}} \frac{1}{|\mathbf{q}| + q_{\text{TF}}} \sum_{\gamma_1,\gamma_2,\gamma_3,\gamma_4} \sum_{\alpha',\beta'} \\ \left(\frac{f_1}{(\epsilon_1 - \epsilon_2)(\epsilon_1 - \epsilon_3)} + \frac{f_2}{(\epsilon_2 - \epsilon_3)(\epsilon_2 - \epsilon_1)} + \frac{f_3}{(\epsilon_3 - \epsilon_1)(\epsilon_3 - \epsilon_2)} \right) \\ \times d_{\alpha\gamma_1}^*(\mathbf{k}) d_{\alpha'\gamma_1}(\mathbf{k}) d_{\alpha'\gamma_4}^*(\mathbf{k} - \mathbf{q}) d_{\beta'\gamma_4}(\mathbf{k} - \mathbf{q}) d_{\beta'\gamma_2}^*(\mathbf{k}) d_{\alpha\gamma_2}(\mathbf{k}) \times (f(\epsilon_4)/2) + (1 \leftrightarrow 2) \\ = \frac{g}{2N^2l^2} \sum_{\mathbf{k},\mathbf{q}} \sum_{\gamma_1,\gamma_2,\gamma_4} \sum_{\alpha',\beta'} \frac{1}{|\mathbf{q}| + q_{\text{TF}}} \times \left(\frac{f_1 - f_2}{(\epsilon_1 - \epsilon_2)^2} + \frac{1}{\epsilon_2 - \epsilon_1} \frac{\partial f_2}{\partial \epsilon_2} \right) \times (f(\epsilon_4)) + (1 \leftrightarrow 2) \\ \times d_{\alpha\gamma_1}^*(\mathbf{k}) d_{\alpha\gamma_2}(\mathbf{k}) d_{\alpha'\gamma_1}(\mathbf{k}) d_{\beta'\gamma_2}^*(\mathbf{k}) d_{\alpha'\gamma_4}^*(\mathbf{k} - \mathbf{q}) d_{\beta'\gamma_4}(\mathbf{k} - \mathbf{q}), \quad (\text{C}\cdot 6)$$

which leads to Eq. (16). $f_1 = f(\epsilon_1)$, $f_2 = f(\epsilon_2)$, $f_4 = f(\epsilon_4)$, $\epsilon_1 = \epsilon_{\gamma_1}(\mathbf{k})$, $\epsilon_2 = \epsilon_{\gamma_2}(\mathbf{k})$, and $\epsilon_4 = \epsilon_{\gamma_4}(\mathbf{k} - \mathbf{q})$. Since $\partial^2 f(\epsilon)/\partial \epsilon^2 > 0$ and $f(\epsilon) > 0$, one finds that $\sum_\alpha g\chi_\alpha^S < 0$.

Applying a method similar to Eq. (C.5), the vertex correction shown by Fig. 3(d) is calculated as

$$g\chi_\alpha^V = \frac{gT^2}{N^2l^2} \sum_{n,n'} \sum_{\mathbf{k},\mathbf{q}} \frac{1}{|\mathbf{q}| + q_{\text{TF}}} \sum_{\gamma_1,\gamma_2,\gamma_3,\gamma_4} \sum_{\alpha',\beta'} \sum_{\beta} \\ G(n, \epsilon_{\gamma_1}(\mathbf{k})) G(n', \epsilon_{\gamma_3}(\mathbf{k} - \mathbf{q})) G(n', \epsilon_{\gamma_4}(\mathbf{k} - \mathbf{q})) G(n, \epsilon_{\gamma_2}(\mathbf{k})) \\ \times d_{\alpha\gamma_1}^*(\mathbf{k}) d_{\alpha'\gamma_1}(\mathbf{k}) d_{\alpha'\gamma_3}^*(\mathbf{k} - \mathbf{q}) d_{\beta\gamma_3}(\mathbf{k} - \mathbf{q}) d_{\beta\gamma_4}^*(\mathbf{k} - \mathbf{q}) d_{\beta'\gamma_4}(\mathbf{k} - \mathbf{q}) d_{\beta'\gamma_2}^*(\mathbf{k}) d_{\alpha\gamma_2}(\mathbf{k}) \\ = \frac{g}{N^2l^2} \lim_{4 \rightarrow 3} \sum_{\mathbf{k},\mathbf{q}} \frac{1}{|\mathbf{q}| + q_{\text{TF}}} \sum_{\gamma_1,\gamma_2,\gamma_3,\gamma_4} \sum_{\alpha',\beta'} \frac{f_1 - f_2}{\epsilon_1 - \epsilon_2} \times \frac{f_3 - f_4}{\epsilon_3 - \epsilon_4} \\ \times d_{\alpha\gamma_1}^*(\mathbf{k}) d_{\alpha'\gamma_1}(\mathbf{k}) d_{\alpha'\gamma_3}^*(\mathbf{k} - \mathbf{q}) d_{\beta'\gamma_4}(\mathbf{k} - \mathbf{q}) d_{\beta'\gamma_2}^*(\mathbf{k}) d_{\alpha\gamma_2}(\mathbf{k}), \quad (\text{C}\cdot 7)$$

which leads to Eq. (17). $f_1 = f(\epsilon_1)$, $f_2 = f(\epsilon_2)$, $f_3 = f(\epsilon_3)$, $\epsilon_1 = \epsilon_{\gamma_1}(\mathbf{k})$, $\epsilon_2 = \epsilon_{\gamma_2}(\mathbf{k})$, and $\epsilon_3 = \epsilon_{\gamma_3}(\mathbf{k} - \mathbf{q})$. In the last equality, we used the fact that the summation with respect to β gives $\epsilon_3 = \epsilon_4$. Note that $[(f_1 - f_2)/(\epsilon_1 - \epsilon_2)] \times [(f_3 - f_4)/(\epsilon_3 - \epsilon_4)] > 0$ due to $f(\epsilon)$ being a monotonically decreasing function with ϵ and that $\sum_\alpha d_{\alpha\gamma_1}^*(\mathbf{k}) \cdots d_{\alpha\gamma_2}(\mathbf{k}) > 0$, suggesting $\sum_\alpha g\chi_\alpha^V > 0$.

References

- 1) For review: H. Seo, C. Hotta, and H. Fukuyama, *Chem. Rev.* **104**, 5005 (2004).
- 2) S. Katayama, A. Kobayashi, and Y. Suzumura, *J. Phys. Soc. Jpn.* **75**, 054705 (2006).
- 3) T. Mori, A. Kobayashi, Y. Sasaki, H. Kobayashi, G. Saito, and H. Inokuchi, *Chem. Lett.* **13**, 957 (1984).
- 4) R. Kondo, S. Kagoshima, and J. Harada, *Rev. Sci. Instrum.* **76**, 093902 (2005).
- 5) H. Kino and T. Miyazaki, *J. Phys. Soc. Jpn.* **75**, 034704 (2006).
- 6) A. Kobayashi, S. Katayama, K. Noguchi, and Y. Suzumura, *J. Phys. Soc. Jpn.* **73**, 3135 (2004).
- 7) K. Kajita, Y. Nishio, N. Tajima, Y. Suzumura, and A. Kobayashi, *J. Phys. Soc. Jpn.* **83**, 072002 (2014).
- 8) N. Tajima, S. Sugawara, M. Tamura, R. Kato, Y. Nishio, and K. Kajita, *EPL* **80**, 47002 (2007).
- 9) N. H. Shon and T. Ando, *J. Phys. Soc. Jpn.* **67**, 2421 (1998).
- 10) S. Katayama, A. Kobayashi, and Y. Suzumura, *Eur. Phys. J. B* **67**, 139 (2009).
- 11) Y. Takano, K. Hiraki, Y. Takada, H. M. Yamamoto, and T. Takahashi, *J. Phys. Soc. Jpn.* **79**, 104704 (2010).
- 12) M. Hirata, Ph.D. thesis, University of Tokyo (2012).
- 13) M. Hirata, K. Ishikawa, K. Miyagawa, M. Tamura, C. Berthier, D. Basko, A. Kobayashi, G. Matsuno, and K. Kanoda, *Nat. Commun.* **7**, 12666 (2016).
- 14) V. N. Kotov, B. Uchoa, and V. M. Pereira, *Rev. Mod. Phys.* **84**, 1067 (2012).
- 15) H. Isobe and N. Nagaosa, *J. Phys. Soc. Jpn.* **81**, 113704 (2006).
- 16) J. C. Ward, *Phys. Rev.* **78**, 182 (1950).
- 17) A. Kobayashi and Y. Suzumura, *J. Phys. Soc. Jpn.* **82**, 054715 (2013).
- 18) G. Matsuno and A. Kobayashi, *J. Phys. Soc. Jpn.* **86**, 04705 (2017).
- 19) Y. Suzumura and A. Kobayashi, *J. Phys. Soc. Jpn.* **80**, 104701 (2011).
- 20) R. R. Guseinov, *Phys. Status Solidi B* **125**, 237 (1984).
- 21) A. A. Abrikosov, L. P. Gorkov, and I. E. Dzaloshinskii, *Methods of Quantum Field Theory in Statistical Physics* (Prentice Hall, Englewood Cliffs, N.J., 1963).
- 22) L. G. Aslamazov and A. I. Larkin, *Sov. Phys. Solid State* **10**, 875 (1968).
- 23) A. Kobayashi, S. Katayama, Y. Suzumura, and H. Fukuyama, *J. Phys. Soc. Jpn.* **76**, 034711 (2007).
- 24) A. Kobayashi, Y. Suzumura, and F. Fukuyama, *J. Phys. Soc. Jpn.* **77**, 064718 (2008).
- 25) N. Tajima, R. Kato, S. Sugawara, Y. Nishio, and K. Kajita, *Phys. Rev. B* **85**, 033401 (2012).
- 26) T. Nishine, A. Kobayashi, and Y. Suzumura, *J. Phys. Soc. Jpn.* **79**, 114715 (2010).